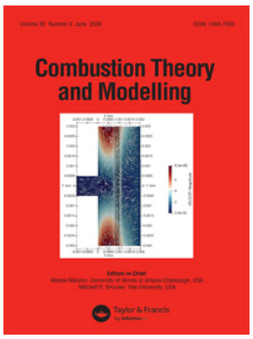

Taylor & Francis
Taylor & Francis Group

Combustion Theory and Modelling

ISSN: 1364-7830 (Print) 1741-3559 (Online) Journal homepage: www.tandfonline.com/journals/tctm20

Linear forcing in physical space for premixed turbulent combustion

Jordan A. Denev , Thorsten Zirwes & Henning Bockhorn

To cite this article: Jordan A. Denev , Thorsten Zirwes & Henning Bockhorn (03 Jun 2026): Linear forcing in physical space for premixed turbulent combustion, Combustion Theory and Modelling, DOI: 10.1080/13647830.2026.2680921

To link to this article: https://doi.org/10.1080/13647830.2026.2680921

Published online: 03 Jun 2026.

Combustion Theory and Modelling, 2026
https://doi.org/10.1080/13647830.2026.2680921

Linear forcing in physical space for premixed turbulent combustion

Jordan A. Denev[a*], Thorsten Zirwes [b] and Henning Bockhorn[c]

[a]*Scientific Computing Center, Karlsruhe Institute of Technology, Karlsruhe, Germany* [b]*Institute for Reactive Flows, University of Stuttgart, Stuttgart, Germany* [c]*Engler-Bunte-Institute, (Combustion Division), Karlsruhe Institute of Technology, Karlsruhe, Germany*

(*Received 28 July 2025; accepted 21 May 2026*)

In the present paper, improvements of the linear forcing method in physical space are developed for both isotropic and anisotropic turbulence. The enhancements achieved are then applied to direct numerical simulations of premixed methane-air flame simulations with inflow-outflow conditions. The first enhancement introduces an individual forcing scheme for each momentum equation, which – unlike previous approaches – removes the constraint that the three space-averaged normal Reynolds stresses must increase or decrease synchronously in time. The second enhancement targets engineering applications involving premixed flames with inflow-outflow conditions. Here, the linear forcing scheme is extended for a flow in a divergent domain, enabling the flame to better stabilise within the computational domain. The third enhancement involves adapting the linear forcing scheme for anisotropic turbulence and applying it to a flame within the divergent domain. Results show that the proposed enhancements – each based on the numerical scheme suggested by Bassenne et al. (2016, Physics of Fluids 28, 035114) – are computationally inexpensive, requiring only 0.26% of the total CPU-time of the simulation. Moreover, it is demonstrated that for anisotropic turbulence, starting from isotropic conditions, the normal Reynolds stresses attain the prescribed levels rapidly, within just one characteristic time interval. When applied to the premixed flame setup, the proposed scheme is used only in the cold, near-inflow region of the domain, which continuously changes shape and size depending on the instantaneous flame position. Results show that with the proposed forcing scheme, the cold volume occupies only a small portion of the domain (11.5–18.0%), demonstrating its numerical efficiency. The consumption flame speed correlates well with the energy dissipation rate (correlation coefficient of 0.86) but negatively with the integral length scale (correlation coefficient of -0.70). Anisotropic turbulence of the same intensity reduces the consumption speed by a factor of 1.11.

Keywords: linear forcing in physical space; divergent domain; anisotropic turbulence; flame stabilisation; direct numerical simulation; flame speed

1. Introduction

The compressible momentum conservation equations, excluding buoyancy forces and second viscosity, can be expressed as:

$$\frac{\partial \rho u_i}{\partial t} + \frac{\partial \rho u_i u_j}{\partial x_j} = -\frac{\partial p}{\partial x_i} + \frac{\partial}{\partial x_j}\left\{\mu\left(\frac{\partial u_i}{\partial x_j} + \frac{\partial u_j}{\partial x_i} - \frac{2}{3}\frac{\partial u_k}{\partial x_k}\delta_{ij}\right)\right\} + \rho S_{Fi} \tag{1}$$

*Corresponding author. Email: jordan.denev@kit.edu

Here, u_i is the value of the velocity component in spatial direction $x_i (i = 1, 2, 3)$, t is time, p is absolute pressure, ρ is density, μ is dynamic viscosity and $\delta_{ij}$is the Kronecker symbol. Summation over repeating indices is implied.

In Equation (1), S_{Fi}represents an additional source term, referred to here as the 'forcing term'. Lundgren [1] was the first to introduce the concept of generating turbulence through this term, proposing the following form:

$$S_{Fi} = Cu_i \tag{2}$$

where C is a constant. This formulation makes the source term linearly proportional to the velocity component u_i, which is why the approach is called 'linear forcing'. The method forces uniformly at all wavenumbers [1]. Considering the balance of the turbulent kinetic energy (TKE) $k = \frac{1}{2}u_i'u_i'$ for statistically stationary isotropic turbulence, Lundgren [1] showed that, assuming isotropic turbulence, the constant C can be expressed in the form:

$$C = \frac{\langle \varepsilon \rangle}{3\left\langle u'^2 \right\rangle} = \frac{\langle \varepsilon \rangle}{\left\langle u_i' u_i' \right\rangle} = \frac{\langle \varepsilon \rangle}{2\,\langle\, k \rangle} \tag{3}$$

where the operator $\langle \cdot \rangle$denotes spatial averaging. Here, ϵ is the dissipation rate of the turbulent kinetic energy, u_i' is the fluctuation of the i^{th} velocity component and u' is the root-mean-square (rms) velocity. According to Equation (3), the forcing constant C represents an eddy turnover time [2].

Over the years, many researchers have contributed to the development of linear forcing in physical space; however, it is not feasible to include all of them here. Therefore, only studies that are directly relevant to the present work and its results will be referenced in the following.

While Lundgren [1] used a pseudospectral code to introduce the concept of linear forcing, Rosales and Meneveau [2] recognised its potential for numerical codes that solve the momentum equation in physical space. In their work, they demonstrated the applicability of this approach for such codes and showed that the results are equivalent to those obtained in spectral implementations. Throughout their simulations, the value of C was kept constant:

$$C = \frac{\varepsilon_\infty}{3u_\infty'^2} \tag{4}$$

which corresponds to a prescribed constant eddy turn-over time-scale. Here, the index '∞' denotes target values to be achieved when approaching statistically steady-state. An important observation in [2] was that the integral length scale, defined as:

$$\ell = \frac{\left\langle u'^3 \right\rangle}{\langle \varepsilon \rangle} \tag{5}$$

is smaller than that obtained from spectral simulations, which typically force in low wavenumber bands, and that it depends on the domain size.

While the above approach is feasible, in large eddy simulations (LES) or direct numerical simulations (DNS), the objective is to attain quasi-steady-state conditions as quickly as possible. Carroll and Blanquart [3] improved the convergence of the turbulent kinetic energy towards the steady state by modifying the forcing term as follows:

$$S_{Fi} = C\frac{k_\infty}{\langle k \rangle}u_i \tag{6}$$

where k_∞ is a target value for the statistically steady-state solution. If, during the iterations, k becomes larger than k_∞, this scheme decreases the source term, and vice versa. According to [3], the use of Equation (6) enables much earlier attainment of statistical stationarity for k compared to the scheme used by [2], while preserving the spectral characteristics of the velocity field.

Noticing that Equation (6) still leads to oscillations of k in time with relative amplitudes of 30 to 40% around the target value, Bassenne et al. [4] developed a forcing method that can reach the desired level of k much faster than the forcing scheme from Equation (6) and then maintain it with less fluctuations during the simulation:

$$C = C(t) = \frac{\langle \varepsilon(t) \rangle - (\langle k(t) \rangle - k_\infty)\, G/t_\infty}{2\,\langle k(t) \rangle} \tag{7}$$

Here, G is a dimensionless constant acting as a proportional gain [4] and t_∞ is an integral time constant, defined as $t_\infty = \frac{u'^2}{\varepsilon}$. In the present study, we use $G = 6.7$, which represents a compromise between stability of the initial iterations (which decreases as G increases) and the degree at which the prescribed value for $\langle k \rangle$ is maintained (which improves with increasing G) during the simulation. Note that C depends only on fluctuating parameters and varies in time, as both $\langle k \rangle$ and $\langle \varepsilon \rangle$ – despite the spatial averaging – also vary with time. For clarity, the notation for time dependence is omitted in the following descriptions.

Up to this point, all considerations have addressed homogeneous isotropic turbulence, typically applied to incompressible flow in a periodic box domain. However, for engineering applications involving inflow-outflow conditions and a turbulent flame within the domain, the method described so far requires specific adaptations and further developments, which are the main focus of this paper. The first contribution of the present work is the extension of the linear forcing scheme from Equation (7), providing greater flexibility by enabling individual forcing of each momentum equation, even in isotropic cases (forcing is done in a way that allows small temporal deviations from the common average rms-value). This topic is addressed in Section 2.

A second contribution of this work is the introduction of a turbulent flame configuration featuring a divergent-shaped domain. This configuration employs inflow-outflow boundary conditions, and the downstream flow deceleration induced by the domain geometry allows the flame to self-stabilise within the computational domain – a task that is challenging to achieve in conventional constant-cross-section geometries. Section 4 presents this configuration and the necessary adaptation of the linear forcing.

The third contribution involves the development of the linear forcing scheme from Equation (7) for cases involving anisotropic turbulence, along with its subsequent application to turbulent flames with anisotropic inflow conditions. The development of the method as well as the corresponding results are presented in Section 5.

2. Individual forcing of the momentum equations at constant turbulent kinetic energy

Although the linear forcing method has been widely adopted for isotropic turbulence – such as in the approaches of [1–4] – these formulations typically assign the same forcing constant C to all three momentum equations, as in the 'forcing at constant turbulent kinetic energy' method of [4], see also Equation (7) above. While this formulation ensures that the overall kinetic energy of the turbulence remains nearly constant over time, it imposes an artificial constraint: the rms values of all three velocity components must either increase or decrease synchronously at each time step, simply following the increase or decrease of the constant C from Equation (7) with time. It is evident that this method is also not suitable for non-isotropic flows.

To address this limitation and facilitate the extension of linear forcing to anisotropic turbulence, an approach similar to those proposed in earlier works [5, 6] is adopted, where forcing is applied individually to each spatial direction. While in [5, 6] the method of [2] was used for individual forcing, the distinctive feature of the present work lies in applying individual forcing to the scheme of Bassenne et al. [4] which has been shown by the authors to accelerate convergence toward statistically steady-state conditions. Specifically, in Equation (7), $\langle k \rangle$ is replaced by the corresponding Reynolds normal stress, resulting in the following modified form:

$$C_1 = \frac{\langle \varepsilon \rangle - \left(\frac{3}{2}\left\langle u_1' u_1' \right\rangle - k_\infty\right) G/t_\infty}{2 \cdot \left(\frac{3}{2}\left\langle u_1' u_1' \right\rangle\right)}; C_2 = \frac{\langle \varepsilon \rangle - \left(\frac{3}{2}\left\langle u_2' u_2' \right\rangle - k_\infty\right) G/t_\infty}{2 \cdot \left(\frac{3}{2}\left\langle u_2' u_2' \right\rangle\right)};$$
$$C_3 = \frac{\langle \varepsilon \rangle - \left(\frac{3}{2}\left\langle u_3' u_3' \right\rangle - k_\infty\right) G/t_\infty}{2 \cdot \left(\frac{3}{2}\left\langle u_3' u_3' \right\rangle\right)} \tag{8}$$

Here, C_1 is the constant for the momentum equation in the $x_1$direction, C_2 for x_2 and C_3 for x_3. Equation (8) allows the turbulence in each of the three momentum equations to evolve independently, while maintaining statistical isotropy on average and ensuring that the value of $\langle k \rangle$ approaches the target value $\langle k_\infty \rangle$. It should be noted that both the dissipation rate $\langle \varepsilon \rangle$ and the normal stresses $\left\langle u_i' u_i' \right\rangle$ in Equation (8) are spatially averaged quantities. The averaging procedure used for the simulation of a turbulent flame is described in Section 4.2.

In the following, the results from Equation (8) are compared with the periodic cubic box domain simulations from [2], where the authors show that by applying forcing in physical space, 'all cases converge to an average scale of about 19% of the domain size' [2]. The case computed using the present forcing method (Equation (8)) corresponds to case 3a (Table 1) from [2], which employs the largest forcing constant and thus generates the strongest turbulence. All simulations in this work are performed with OpenFOAM [7], employing fourth-order interpolation schemes for spatial derivatives and second order implicit schemes for time integration. Because of this, the grid resolution is chosen to resolve the Kolmogorov length with 1.5 to 2 cells, which is three to four times higher than the recommendation by Pope [8] and in line with the recommendation by Moin [9]. The present simulation was initialised with a random velocity distribution. With a domain size of 2π metres, a kinematic viscosity of 4.491×10^{-3} m^2/s, and input parameters $k_\infty = 0.66$ m^2/s^2 and $t_\infty = 1.895$ s in Equation (8), the simulation was performed on a 128^3 grid. The time-averaged results obtained for the integral length scale ℓ are 1.253 m, or 19.94% of the

Table 1. Results of the statistical quantities. Numbers in parentheses denote the target values.

Case	Method	Domain & grid cells	$u'_{1,rms}$ m/s	$u'_{2,rms}$ m/s	$u'_{3,rms}$ m/s	k m^2/s^2	ε m^2/s^3	ℓ mm
1	Present Isotropic	Rectangular10 Mio	0.844(0.85)	0.839(0.85)	0.838(0.85)	1.060(1.08)	868	0.703
2	[4] Isotropic	Rectangular10 Mio	0.914(0.85)	0.804(0.85)	0.801(0.85)	1.066(1.08)	773	0.806
3	Present Isotropic	Divergent10 Mio	0.846(0.85)	0.840(0.85)	0.804(0.85)	1.063(1.08)	830	0.735
4	Present Isotropic	Divergent163 Mio	0.905(0.85)	0.887(0.85)	0.892(0.85)	1.205(1.08)	2700	0.282
5	Present Anisotropic	Divergent20 Mio	1.123(1.20)	0.646(0.60)	0.629(0.60)	1.038(1.08)	925	0.631

domain length, confirming that the present method predicts the correct integral length scale with the required precision for canonical flows such as periodic cubic box turbulence.

A further comparison with the results of [2] shows that the present turbulence is fully isotropic, with average rms-values in each spatial direction $u'_{1,rms} = 0.66285$, $u'_{2,rms} = 0.66271$, and $u'_{3,rms} = 0.66269$ m/s, which closely match the target value of 0.6633 m/s. The energy dissipation rate, $\epsilon = 0.236\,\mathrm{m}\supset 2/\mathrm{s}^3$, is 1.12 times higher than that reported by [2] ($\epsilon = 0.210\,\mathrm{m}\supset 2/\mathrm{s}^3$). It should also be noted that ϵ is considerably lower here compared to the inflow-outflow setups discussed in the next section.

3. Application to flows with inflow-outflow boundaries

Bearing in mind the ultimate goal of simulating turbulent flames in domains with a divergent shape and inflow-outflow boundary conditions, this and the following sections apply the proposed forcing scheme to a sequence of flow configurations that progressively approach this target. As a first step, the present method is applied to a rectangular domain with inflow-outflow boundary conditions and compared with the approach described in [4].

3.1. *Rectangular domain with inflow-outflow boundary conditions*

The geometry of the considered rectangular isothermal flow with periodic boundaries along the y and z directions is shown in Figure 1(a,b). The black line at the sides indicates the downstream end of the forcing zone, set at x = 3.75 mm to match the subsequent combustion simulations. For the same reason, the domain dimensions are defined as $8.96 \times 7.88 \times 7.88$ mm, corresponding to the same volume as the divergent domain discussed in the next subsection. The structured numerical grid consists of over 10 million rectangular cells ($256 \times 200 \times 200$), and the inflow velocity was 1.0 m/s. The flow was initialised with a uniform velocity of 1.0 m/s. In all simulations without a flame, the value G = 67 was used to strongly force the turbulence toward the target TKE level, thereby enabling consistent comparison between them. The constant t_∞ was set to 0.00206 s for consistency with the combustion simulations described in Sections 4 and 5. The kinematic viscosity was set to the same value as in the cold region of the flame simulations, namely $\nu = 16.25 \times 10^{-6}$ m^2/s.

Table 1 shows the statistical results from the two simulations: the present method based on Equation (8) (case 1) and the approach of [4] based on Equation (7) (case 2). The values in this table represent time-averaged quantities obtained after spatial averaging was

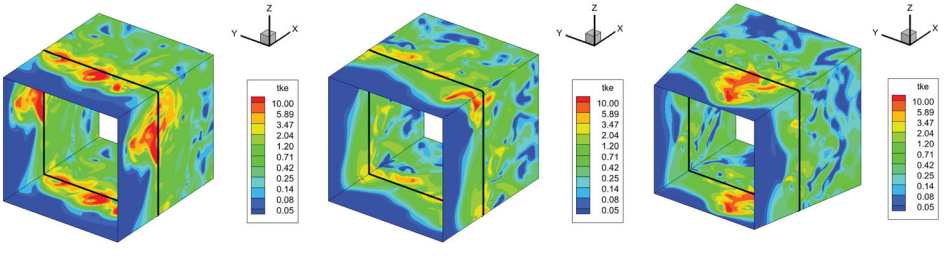

a) Rectangular (Eq. (8)) b) Rectangular [4] (Eq. (7)) c) Divergent (Eq. (8))

Figure 1. Geometry and a time snapshot of the turbulent kinetic energy (TKE) in the rectangular and divergent flow configurations.

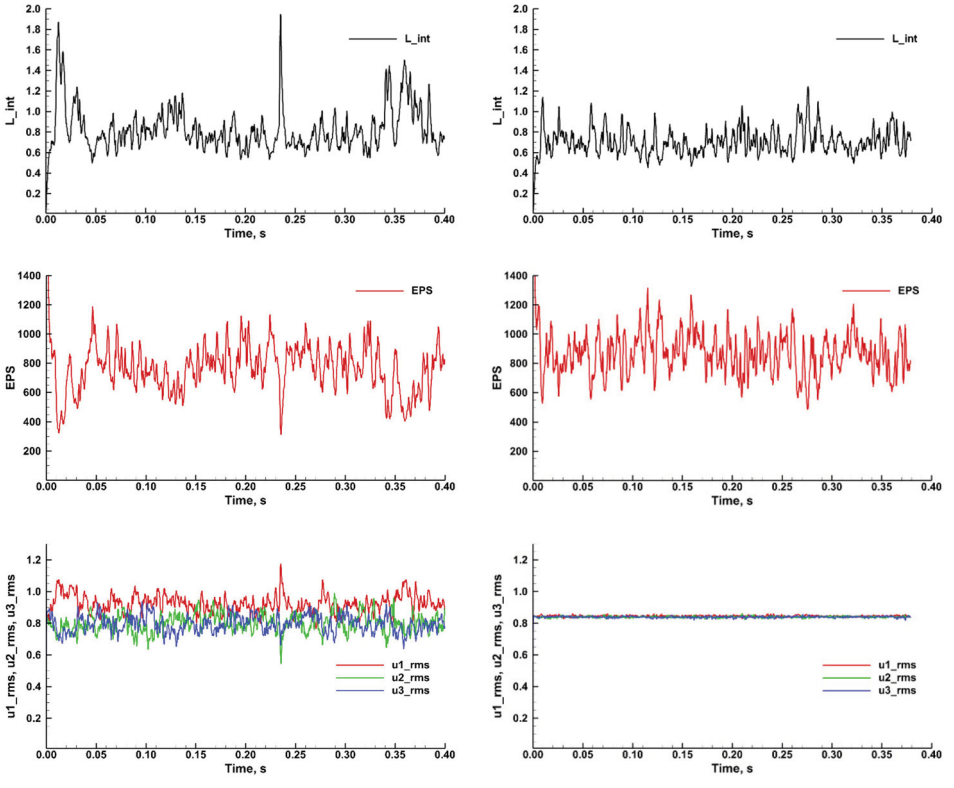

Figure 2. Integral length scale, energy dissipation rate and rms of velocity components for the method of [4] (case 2, on the left-hand side) and the present method (case 1, on the right-hand side).

performed and recorded at each time step. Figure 2 presents the time evolution of the statistical quantities for the two cases. Case 3 from Table 1 is introduced in Section 3.2, case 4 is considered in Section 4, and case 5 is addressed in Section 5. The numbering of the cases is consistently maintained across the following tables in this paper.

As expected from the similarity between Equations (7) and (8), both methods produce statistical values for this rectangular domain that, although not identical, are quite close to each other. Let us begin with the integral length scale ℓ. The method of [4] yields values about 1.15 times higher, which corresponds to the lower energy dissipation rate ε obtained with this method. Both quantities are compared in Figure 2. It can be observed that the method of [4] shows temporarily higher peaks for ℓ, whereas the results from the present method are more constrained. As evident from Figure 2, in the present model the dissipation rate reaches its steady-state level somewhat faster.

Essentially, the presence of a strong convective downstream flow results in turbulence characteristics that no longer correspond to those of the periodic cubic box investigated in [2] as well as at the end of Section 2. As shown in Table 1, the energy dissipation rate for both methods is on the order of 10^2, whereas that in [2] equals 0.210 m⊃2/s³, i.e. on the order of 10^{-1}. Furthermore, taking the hydraulic diameter as the natural reference length scale for flows with inflow-outflow boundary conditions, the integral length scale obtained by the method of [4] corresponds to 10.2% of the hydraulic diameter, while that from the present method is 8.9%. Both results differ substantially from the 19% obtained for the

periodic cubic box and essentially represent outcomes determined by the simulation setup rather than a priori known values.

A possibility for comparison with the present results is provided by Nilsson et al. [10], who studied a flame in a rectangular domain using a low-wavenumber forcing method described in [11]. For a case with $u'/S_{L0} = 15$ (premixed methane flame, equivalence ratio $\phi = 0.6$, grid resolution $\Delta x = 10\,\mu m$; S_{L0} stands for the unstretched laminar flame speed) they report an integral length scale $\ell = 0.68\,mm$, which agrees well with the values from this study (see Table 1).

Further analysis shows that although both methods (present and from [4]) yield turbulent kinetic energy values close to the target value of $1.08\,m^2/s^2$, the present method produces more uniform – i.e. more isotropic – rms values than the method of [4], for which $u'_{1,rms}$is 1.14 times higher than $u'_{3,rms}$. The stronger uniformity of the present method is also evident from Figure 2. A plausible explanation for this behaviour is that the present method independently controls each rms component ($u'_{1,rms}, u'_{2,rms}, u'_{3,rms}$), whereas the method of [4] lacks a mechanism for such independent control, as it directly forces the sum of the components – namely, the turbulent kinetic energy itself.

In the following, the two methods (present method and from Bassenne et al. [4]) are compared in terms of their numerical characteristics, with the corresponding results summarised in Table 2. Each simulation was performed on 128 CPU cores over a period of 24 h and the time step was guided by fixing the CFL number to 0.9 [12]. The results show that the present method exhibits a slightly smaller time step and reaches a shorter physical simulation time than the method of [4]. The CPU time required to compute the forcing constants from Equations (7) or (8), the cold-domain averaged values of TKE, RMS velocity components, and energy dissipation rate – for all cases in Table 2 – is quite low, ranging from 1.3% to 1.4%. This demonstrates the method's overall effectiveness.

Furthermore, for all cases in Table 2, the Kolmogorov length scale η is larger than the smallest grid size (near the inflow), indicating that the grid resolution is sufficiently fine to resolve even the smallest turbulent structures.

In conclusion, both methods [4] and the present one deliver results that are close to each other. The present method is slightly slower in its overall performance (it advances to a physical end time that is 9% shorter) than the method of [4]. However, for the isotropic case considered, the present results are fully isotropic, while the method of [4] shows a difference of a factor of 1.14 between the individual RMS values of the velocity components.

3.2. *Flow in a divergent domain*

The next step towards a flame simulation is to examine the performance of the proposed method for isothermal flow in a divergent domain. The divergent domain geometry is shown in Figure 1(c); structured hexahedral numerical grid is applied. Its domain volume equals that of the two rectangular domains. While other technical details for the divergent geometry can be extracted from the following sections, here the primary goal is to compare the turbulent and numerical characteristics with those of the rectangular geometries. Therefore, all simulation parameters are set identical to those of the rectangular flows from the previous subsection.

A first impression of the results can be gained by comparing the instantaneous turbulent kinetic energy shown in Figure 1. It can be seen that the TKE results here are qualitatively and quantitatively quite close to those from the two rectangular domain simulations.

Table 2. Numerical characteristics of the incompressible flows with inflow-outflow boundary conditions. The last column shows the grid size near the inflow and the Kolmogorov length scale η (in parentheses). The number of time steps reached for 24 h on 128 CPU cores.

Case	Method	Domain shape & Grid cells	Physical time reached & % CPU time	Number of time steps –	Average time step, Δt	Grid size and η
1	Present Isotropic	Rectangular10 Mio	0.379 s1.347%	127 328	2.98E-06 s	35 µm(47 µm)
2	[4] Isotropic	Rectangular10 Mio	0.417 s1.316%	125 606	3.32E-06 s	35 µm(48 µm)
3	Present Isotropic	Divergent10 Mio	0.387 s1.388%	120 596	3.21E-06 s	35 µm(48 µm)

Further time-averaged results are presented in Tables 1 and 2 (case 3). These show that the results for the divergent domain – both turbulence characteristics and numerical parameters – lie between those of the two rectangular domain simulations for all investigated time-averaged quantities.

4. Linear forcing of a premixed flame with isotropic turbulence

4.1. *Geometry of the divergent domain and flame stabilisation*

In domains with inflow-outflow boundary conditions and a constant cross-sectional area, flames often migrate downstream, moving forth and back. This unsteady behaviour results from fluctuations in turbulence intensity, which cause the flame speed to vary locally. Hence, over extended simulation times, these fluctuations may cause the flame to flash back or abruptly leave the computational domain. These challenges are especially pronounced when using very fine computational grids, as they demand considerable resources, including prolonged downstream domains. For instance, [13] reports simulations for which the domain is up to six times longer in the downstream direction than in the lateral directions.

To mitigate these issues, the divergent domain configuration is introduced and utilised, see Figure 3. The basic idea of the divergent domain geometry follows practically established configurations of radial or conical porous burners: in such physical devices, the flame stabilises at a position where its burning velocity equals the velocity of the incoming fresh gas mixture [14]. Following this basic principle, the present simulation of a lean, premixed methane-air flame employs a divergent domain to enable the flame to self-adjust its position. As the velocity decreases along the streamwise distance, the flame can stabilise at a location where its propagation speed matches that of the local flow, thus remaining entirely within the computational domain. Flashback is prevented by setting the inflow velocity near the inlet significantly higher than any possible flame speed, even under high turbulence. Similarly, the flame is unlikely to exit the computational domain downstream

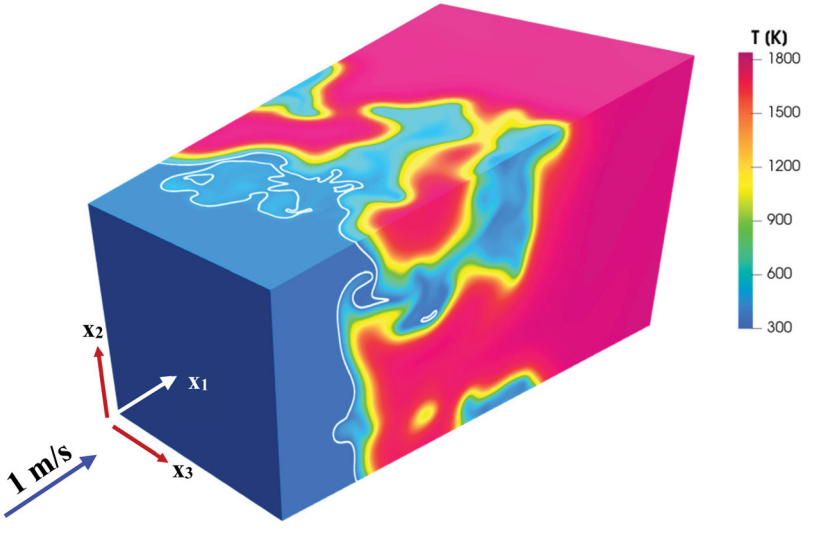

Figure 3. Geometry of the divergent domain with temperature distribution. The white line marks the boundaries of the 'cold' inflow region, where forcing is applied.

because, if it approaches the outlet, the fresh gases (before being influenced by the flame) will have a sufficiently low velocity to allow the flame to propagate back into the domain. Thus, with an appropriate choice of both the expansion angle and the inflow velocity, the divergent domain setup provides the flame with the flexibility to self-adjust its position—even over relatively long simulation times. Geometrical features of the domain and the structured numerical grid are presented in Tables 3 and 4.

A lean methane-air mixture with equivalence ratio $\phi = 0.7$and temperature 300 K enters the domain at $x_{1,min} = 0$m with a constant (both spatially and temporally uniform) speed of 1.0m/s in x_1-direction. Periodic boundary conditions are applied in both spanwise directions of the computational domain. The flow, which enters the domain in a laminar state, becomes turbulent downstream due to the linear forcing method applied here. The u_1-velocity component is first initialised with the laminar velocity field, which varies along $x_1$and is determined from the continuity equation under the assumption of incompressible flow. For the first time step, random numbers with a uniform distribution in the range $[-0.5, 0.5]$ are superimposed on this laminar velocity field.

Chemical reactions within the flame are initialised by imposing a temperature of 1900K at locations where $x_1 > 5$mm. The reaction mechanism used is that by Kee [15], comprising 17 species and 58 reactions. The corresponding laminar flame speed of the $\phi = 0.7$ methane-air flame is $S_{L0} = 0.1938$m/s, and the thermal flame thickness is $\delta = 0.66$mm. All combustion simulations have been performed with the in-house code EBI-DNS [16], which couples OpenFOAM [7] and Cantera [17] to solve the compressible Navier-Stokes equations and mass and energy balances including chemical reactions. Fourth-order interpolation schemes were applied for spatial discretisation, and a second-order implicit scheme for time derivatives. In the same way as for the incompressible cases, Table 4 shows that the grid resolution for the combustion simulations is 1.5 to 2 times smaller than the Kolmogorov length scale. Additionally, the flames are resolved with 20 to 40 grid points, exceeding the recommendation by Poinsot and Veynante [18] by a factor of two to four. The CFL number is fixed to 0.2.

4.2. *Adapting the divergent domain configuration for a flame simulation*

For the divergent domain configuration described above, the linear forcing method requires specific adaptations. The first concerns the region where forcing is applied. Following the approach of Klein et al. [19], forcing in this work is restricted to the 'cold' domain. The cold domain forcing is employed here for two reasons: first, to avoid directly affecting the flame front through the forcing, and second, to prevent turbulence decay that could occur if the turbulence was imposed as a boundary condition exactly at the inlet. With the aim to maintain nearly constant physical quantities such as density and dynamic viscosity, a temperature threshold of 330 K is used to distinguish between the 'cold' (forced) and 'hot' (not forced) parts of the domain. In Figure 1, this threshold is indicated by the thick white line.

The second adaptation addresses the calculation of fluctuating velocities in the divergent domain configuration. In classical box turbulence simulations with periodic boundaries, the mean velocity in any spatial direction is zero, so Equation (2) or Equation (8) is applied directly to the velocity fluctuations. However, in inflow-outflow setups, applying forcing to the instantaneous velocities would cause the mean flow direction to dominate, resulting in excessive forcing along that axis. To avoid this, the time-averaged velocity is first subtracted from the instantaneous velocities, and Equation (8) is then applied solely to the

Table 3. Domain lengths and number of cells for the combustion simulations.

Case	Turbulence	$\mathbf{L}_{\mathbf{x}1}$ mm	$\mathbf{L}_{\mathbf{x}2,\,\mathbf{x}3}$ at $\mathbf{x}_{1,min}$ mm	$\mathbf{L}_{\mathbf{x}2,\,\mathbf{x}3}$ at $\mathbf{x}_{1,max}$ mm	Grid cells $\mathbf{N}_{\mathbf{x}1}$	Grid cells $\mathbf{N}_{\mathbf{x}2} = \mathbf{N}_{\mathbf{x}3}$	Total number of grid cells
4	Isotropic	17.92	7.0	10.5	1024	400	163 840 000
5	Anisotropic	17.92	7.0	10.5	512	200	20 480 000

Table 4. Grid resolution and Kolmogorov length for the combustion simulations.

Case	Turbulence	Grid resolution along $\boldsymbol{x}_1$ µm	Grid resolution along $\boldsymbol{x}_2, \boldsymbol{x}_3$ µm	Grid cells per flame thickness $\boldsymbol{\delta}$ –	Energy dissipation rate ϵ m^2/s^3	Kolmogorov length η (cold domain) µm
4	Isotropic	17.50	17.50-26.25	25–38	2700	35.51
5	Anisotropic	35.00	35.00-52.50	12–19	925	46.41

fluctuations. It is worth noticing that for the divergent domain configuration – where the downstream velocity continually decreases (considering only the cold region) – the local time-averaged velocity along the x_1 direction is obtained from the continuity equation. This ensures that forcing does not become disproportionately strong in the main flow direction.

For the lateral velocity components, the spatial average within the cold domain is calculated at each time step and subtracted from the instantaneous velocity before applying the linear forcing. This ensures that any occasionally arising strong flow in a lateral direction will be damped rather than amplified. Turbulence statistics, such as the domain-average turbulent kinetic energy k, are calculated after the average velocity has been subtracted.

For Equation (8), the parameters of interest are k_∞ and t_∞. The first one represents the target value for the turbulent kinetic energy in the 'cold' domain – after statistically steady-state conditions are reached. In this study, it was set to $k_\infty = 1.08\text{m}^2/\text{s}^2$ and corresponds to an rms-value of $u' = 0.85\text{m/s}$. The second parameter represents a timescale, set to $t_\infty = 0.00206$ s. This value was determined using Equation (5) and 19% of the hydraulic diameter at the divergent domain's midsection, following the observation in [2]. Note that this timescale – once forcing reaches steady state and the bracketed term in Equation (8) approaches zero – does not influence the results. This completes the computation of the constants in Equation (8) for the proposed linear forcing method.

The flow with the premixed flame was first initialised and then simulated for 0.1 s to reach statistically steady-state conditions. Subsequently, an additional 0.0615 s of simulation was performed for evaluation purposes; only this period is presented in the results section, with the time axis shifted for convenience to start from 0.0 s. The evaluation period spans 30 times the timescale presented above and is therefore sufficiently long.

We note that no additional filtering is applied to the fluctuating velocities in the present study – a technique that could control the integral length scale, as demonstrated in [6, 19, 20]. However, this work focuses on evaluating linear forcing alone, without introducing extra parameters or modifications to Equations (8) or (9).

4.3. *Results from the lean premixed methane-air flame simulation – isotropic turbulence*

As a first step, the volume of the cold region – subjected to linear forcing – is examined over time. Figure 4(a) shows that the volume of this region remains nearly constant, which is a prerequisite for maintaining a stable flame position that does not fluctuate significantly. The cold region volume, depicted in Figure 4(b), varies between 11.5% and 18.0% of the total domain volume. Expressed in terms of the variation of the x_1-coordinate of the cold region boundary (defined as $\text{T} = 330\,\text{K}$), this means that the average x_1-coordinate of the boundary remains within the range of 3mm to 4.51mm throughout the simulation. Figure 4(b) illustrates the evolution of the turbulent kinetic energy from the laminar inflow boundary condition to downstream levels that ensure the space-averaged TKE in the cold domain is maintained at $k_\infty = 1.08\text{m}^2/\text{s}^2$.

Figure 5 presents the individual rms values of the velocity components along with the corresponding turbulent kinetic energy (TKE). The mean rms velocities according to the three spatial directions are $u'_{1,rms} = 0.905$, $u'_{2,rms} = 0.887$, and $u'_{3,rms} = 0.892\,\text{m/s}$, respectively. These similar values indicate that the forcing scheme from Equation (8) produces the desired isotropic turbulence (on average), while temporarily allowing each velocity fluctuation to vary independently up or down, see Figure 5. This is the key difference from the method proposed by Bassenne et al. [4] (see Equation (7)), which requires all fluctuations

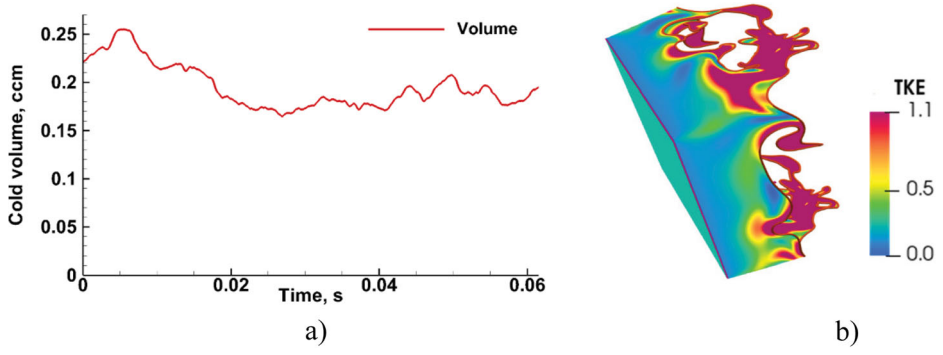

Figure 4. The cold region in which the forcing is applied: (a) Cold region volume as a function of time. (b) The cold region volume shown on the domain boundaries and coloured by the TKE.

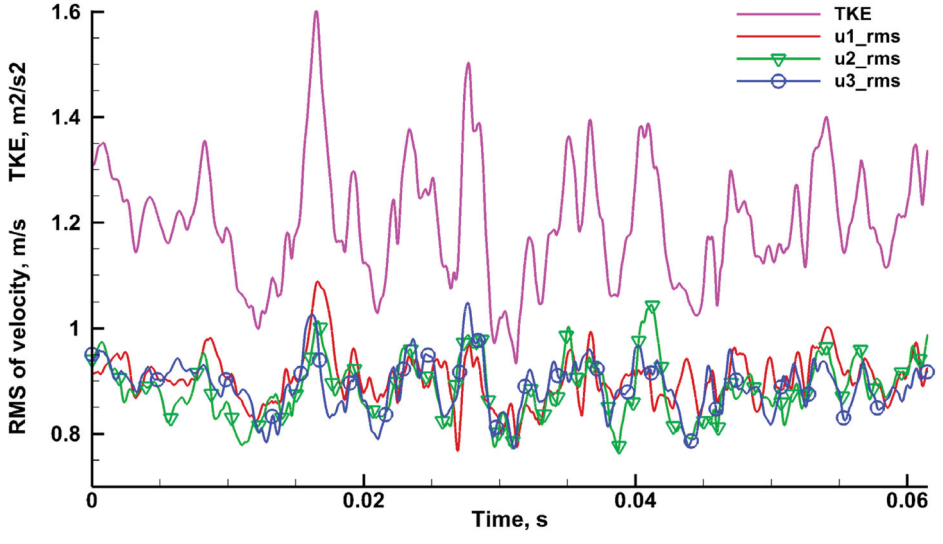

Figure 5. Rms of the velocity fluctuations as well as of the TKE over time. The values presented are spatial averages over the cold domain ($T \leq 330$K).

to increase or decrease synchronously. All three velocity fluctuations are slightly higher than the prescribed value of 0.85 m/s. Consequently, the average TKE is 1.20 m⊃2/s⊃2, somewhat above the target value of 1.08 m⊃2/s⊃2.

Figure 6 shows the flame consumption speed alongside the energy dissipation rate of turbulent kinetic energy and the integral length scale. Notably, the flame speed exhibits a strong positive correlation with the dissipation rate, ϵ, as clearly seen in the figure; the correlation coefficient is 0.86. Conversely, the flame speed is also correlated with the integral length scale, but negatively, with a correlation coefficient of -0.70 (due to the opposing correlation between ϵ and ℓ from Equation (5)).

The average value of the dissipation rate, ϵ, over the time interval shown in Figure 6 is 2700 m⊃2/s³; please note that the dissipation rate was not controlled in any way in the present study and the obtained value is simply the result from the simulation. The relatively high dissipation rate ϵ is attributed to linear forcing acting directly on the smallest scales in

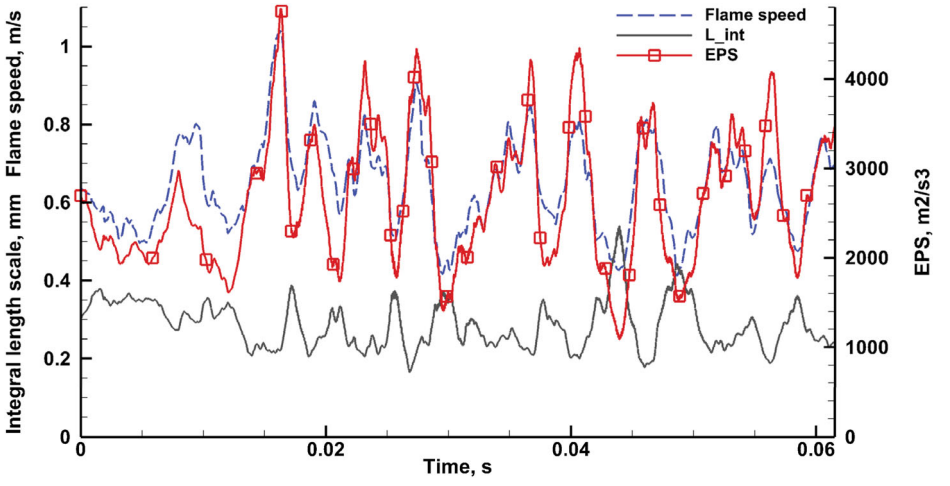

Figure 6. Energy dissipation rate, integral length scale (both averaged over the cold domain) and consumption flame speed.

physical space. Since ϵ is computed from derivatives at the smallest grid scales, it directly reflects the forcing impact. This high dissipation – in the denominator – yields correspondingly low integral length scales, resulting in smaller turbulent Reynolds numbers. For the current simulation, the obtained length scale in the cold region is $\ell = 0.282$ mm (c.f. Table 1, Case 4) and the turbulent Reynolds number, defined as $Re_t = \frac{\ell u'}{\nu} = \frac{u'^4}{\nu\varepsilon}$,is equal to 15.2.

Table 4 (case 4) presents the grid size and Kolmogorov length scale, where the grid size is considerably smaller than the Kolmogorov length scale. In the cold domain of primary interest – where the spanwise grid is twice as fine as the Kolmogorov scale – the resolution is adequate to resolve even the smallest turbulent eddies.

The CPU time required to compute the additional quantities – such as the space-averaged values over the cold domain – along with the source terms in Equation (8), has been measured. The time spent computing these additional quantities for linear forcing accounts for only 0.26% of the total simulation time – about five times lower than for incompressible simulations (cf. Table 2). This demonstrates the method's computational efficiency and suitability for resource-intensive approaches like highly resolved Large Eddy Simulation (LES) or Direct Numerical Simulation (DNS).

5. A flame simulation with anisotropic turbulence

5.1. *Extending the present forcing to anisotropic simulations*

Up to now, the proposed forcing scheme has been tested and compared with the method of [4] for cases of isotropic turbulence. However, the inherent ability of the present method to control each velocity component individually and independently provides a natural basis for applications involving anisotropic turbulence. To start with the anisotropic scheme, let us first review the work of [5], which introduced a general forcing method for Large Eddy Simulations (LES) and demonstrated its application to both LES and hybrid LES/Reynolds-Averaged Navier-Stokes frameworks. This method, referred to as anisotropic linear forcing, is based on an unsteady linear tensor function of the resolved

velocity field. Implementing this approach requires the calculation of additional statistical quantities, including the principal invariants of the Reynolds stress tensor, as well as the solution of a second-order tensorial algebraic equation to determine the coefficients for linear forcing. Therefore, from now on, the work from previous sections will be extended by adapting the present forcing scheme to cases of anisotropic turbulence.

To begin the adaptation to homogeneous anisotropic turbulence, it should be noted that Equation (8) – obtained by substituting k from Equation (7) with $\frac{3}{2}\langle u_1' u_1' \rangle$ – thereby allowing each momentum conservation equation to independently set its own level of velocity fluctuations – still implicitly retains the assumption of isotropic homogeneous turbulence. Therefore, to develop the anisotropic forcing, Equation (7) is taken as the starting point. To clarify how anisotropy is introduced into the system, consider the following example: suppose the RMS values of the velocity fluctuations are intended to be twice as large in the direction of the flow (index 1) compared to the two lateral directions:

$$u_{1,rms}' = 2 \cdot u_{2,rms}' = 2 \cdot u_{3,rms}' \text{ or } \left\langle u_1' u_1' \right\rangle = 4 \cdot \left\langle u_2' u_2' \right\rangle = 4 \cdot \left\langle u_3' u_3' \right\rangle$$

In this way, the turbulent kinetic energy k can be expressed independently in terms of each individual Reynolds normal stress:

$$\langle k \rangle = \frac{\left(\langle u_1' u_1' \rangle + \langle u_2' u_2' \rangle + \langle u_3' u_3' \rangle\right)}{2} = \frac{3}{4}\left\langle u_1' u_1' \right\rangle = 3\left\langle u_2' u_2' \right\rangle = 3\left\langle u_3' u_3' \right\rangle \tag{9}$$

As the next step, the expressions from Equation (9) are substituted into Equation (7), resulting in the following source terms for the momentum equations:

$$\begin{aligned} C_1 &= \frac{\langle \varepsilon \rangle - \left(\frac{3}{4}\langle u_1' u_1' \rangle - k_\infty\right) \mathrm{G}/t_\infty}{\frac{3}{2}\langle u_1' u_1' \rangle}; \\ C_2 &= \frac{\langle \varepsilon \rangle - \left(3\langle u_2' u_2' \rangle - k_\infty\right) \mathrm{G}/t_\infty}{6\langle u_2' u_2' \rangle}; \\ C_3 &= \frac{\langle \varepsilon \rangle - \left(3\langle u_3' u_3' \rangle - k_\infty\right) \mathrm{G}/t_\infty}{6\langle u_3' u_3' \rangle} \end{aligned} \tag{10}$$

The expressions in Equation (10) enable individual forcing of the momentum equations while maintaining the kinetic energy $k$nearly constant and approaching the target value $k_\infty = 1.08\mathrm{m}^2/\mathrm{s}^2$ – which was chosen to be the same as in the isotropic case.

The algorithm proposed above is primarily suitable for cases in which the ratio between the rms values of the individual stresses from Equation (9) remains constant both throughout the forcing region and over time. For most simulations, this condition is satisfied.

5.2. *Anisotropic flame simulation results*

In this section, the relations from Equations (9) and (10) are used to investigate the anisotropic forcing as well as the transition from isotropic to anisotropic turbulence. The starting point is a fixed time-step from the flame simulation of isotropic turbulence presented in Section 4.3. To accelerate the computations, results from the fine numerical grid (case 4 in Table 3) are interpolated onto a grid coarsened by a factor of two (case 5 in

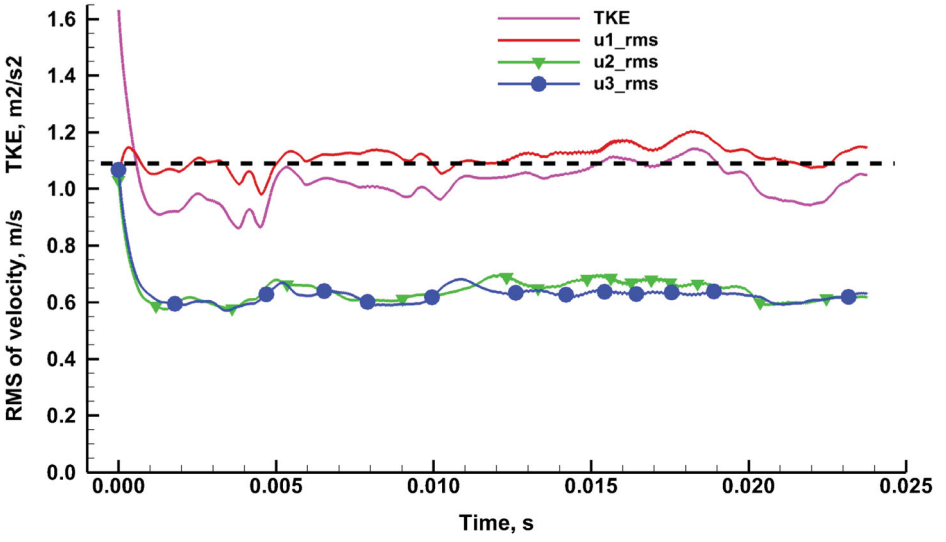

Figure 7. Anisotropic forcing: TKE and RMS velocity fluctuations.

Table 3). The simulation then continues on the coarser grid – with the forcing scheme from Equation (10) – for additional 0.024 seconds. During the simulations, the space-averaged turbulence properties of the cold forcing region are monitored over time. Figure 7 presents the rms values of the velocity components as well as the resulting turbulent kinetic energy in this region.

It can be observed that anisotropy is already established after one characteristic time of 0.00206 s; the statistical evaluation presented below is conducted for the time interval following this point. As shown in the figure, the turbulent kinetic energy does not reach its target value ($1.08\text{m}^2/\text{s}^2$), indicated by the dashed line; instead, its average value remains slightly lower at $1.038\text{m}^2/\text{s}^2$. The average values for $u'_{2,rms}$ and $u'_{3,rms}$ are 0.646m/s and 0.629m/s, respectively. These values are intended to be 0.60m/s, i.e. half of the $u'_{1,rms}$ value, see Table 1 (case 5); however, the ratio 1:2 is not fully achieved, as the average $u'_{1,rms}$ value – measured at 1.123m/s – is itself underpredicted. This underprediction is related to the lower kinetic energy observed. As a whole, the achieved anisotropy, calculated as $0.638/1.123 = 0.568$ (with 0.638 being the average spanwise velocity rms), differs from the expected value of 0.500 by a factor of 1.136, but still represents a clearly anisotropic turbulence. The anisotropy could be increased further by choosing a larger value of the control constant G.

Let us compare the values of ε and ℓ with those from the cold divergent domain case (case 3, Table 1), which has the same grid resolution as the present simulation (case 5, Table 1). Note that in the present simulation, the forcing domain is not fixed but changes dynamically over time, similarly to the domain shown in Figure 4(b). The comparison shows that the dissipation rates for the two cases are quite close, with the present ε being only 1.11 times higher than in the cold simulation with a fixed forcing region. This confirms the method's robustness and repeatability, even for the more complex case of an anisotropic premixed flame simulation. Table 4 (case 5) shows that the grid resolves the Kolmogorov length scale with more than one cell in the cold region near the inflow. In the hot region affected by the flame, increased viscosity further enlarges the Kolmogorov scale.

Next, we examine the consumption flame speed and compare it with that from the isotropic turbulence case considered in Section 4 (case 4 in the tables). The present averaged consumption speed is 0.588 m/s, compared to 0.653 m/s in the isotropic case (case 4 in the tables). An interesting result is that anisotropic turbulence – with downstream fluctuations nearly twice the lateral ones – leads to less flame folding and thus reduces the consumption speed by a factor of 1.11.

6. Conclusions

In this work, the linear forcing method in physical space is extended and applied to both isotropic and anisotropic turbulent flows interacting with a premixed methane-air flame. The proposed method builds on the constant turbulent kinetic energy (TKE) forcing scheme of Bassenne et al. [4], which the authors have demonstrated to be numerically efficient. The essence of the current developments lies in the individual control of the forcing for each momentum equation, which enables its natural extension to anisotropic turbulence.

To ensure flame stability and containment within the computational domain, a divergent domain configuration with inflow-outflow boundary conditions is introduced and adapted for the linear forcing approach of premixed turbulent flames. The method is first tested and applied to several incompressible flows with simpler rectangular geometries that progressively approach the divergent domain configuration. Validation against the periodic box setup from [2] confirms that it accurately reproduces the integral length scale (19.94% of the domain length), energy dissipation rate, and targeted TKE.

As a next step, the results from a rectangular incompressible flow are compared with those from the original method of [4], showing good agreement for both numerical and physical quantities. Small differences still exist – for instance, for this isotropic turbulence case, the method of [4] is computationally more efficient, but the present method yields a noticeably more isotropic solution. Finally, an incompressible divergent domain flow is compared to the two rectangular domain flows, demonstrating that the case with the divergent shape yields quantitatively and qualitatively very close results.

The divergent domain configuration demonstrates its main advantage in combustion simulations by allowing the flame to self-adjust its position, preventing flashback or blowout. For premixed turbulent combustion, linear forcing is applied only in the cold region ($T < 330\,K$), which varies dynamically due to the movement of the flame and the intense turbulent mixing. In the isotropic combustion case, this forced cold fresh gas region occupies 11.5%–18% of the total volume, providing ample space for flame development. The divergent shape, combined with the relatively small changes in the forced volume size, stabilises the flame's position within the computational domain.

The present extension of the linear forcing method is numerically efficient, consuming less than 1.4% of total CPU time for all incompressible flows. In the combustion case – with a fine grid of 163 million cells, 17 species, and 58 chemical reactions – this fraction dropped further to just 0.26% of total simulation time, confirming the suitability of the method for high-performance computing.

All simulations use a structured hexahedral grid with resolution at or below the Kolmogorov length scale (see Tables 2 and 4). While the method actively controls turbulent kinetic energy (TKE) levels, the average dissipation rate emerges as a simulation outcome. Notably, in the combustion simulation under isotropic turbulence,

this dissipation rate correlates strongly with the flame consumption speed (correlation coefficient = 0.86).

The anisotropic combustion case was initiated from the interpolated isotropic case. However, the simulation rapidly reached the targeted anisotropic state – within one integral time scale (0.00206 s) – thus demonstrating once again the method's numerical efficiency. The flame under anisotropic turbulence experiences less front folding and thus exhibits a consumption speed (0.588 m/s) that is 1.11 times smaller than in the isotropic case.

Overall, this work advances the linear forcing method of [4] for premixed turbulent flames interacting with isotropic or anisotropic turbulence. Engineering scenarios with inflow-outflow boundary conditions benefit from the divergent domain geometry, which enables the flame to naturally adjust its position while remaining confined within the computational domain – thus shortening its length and saving CPU time in high-performance computing applications.

Future work will integrate the present developments with methods for independently controlling both turbulent kinetic energy (TKE) and integral length scale – as proposed in [6, 19, 20] – and adapt this approach for simulating turbulent premixed flames.

Author contributions

CRediT: **Jordan A. Denev:** Conceptualization, Investigation, Methodology, Software, Validation, Visualization, Writing – original draft; **Thorsten Zirwes:** Investigation, Methodology, Software, Validation, Writing – review & editing; **Henning Bockhorn:** Conceptualization, Methodology, Project administration, Supervision, Writing – review & editing

Disclosure statement

No potential conflict of interest was reported by the author(s).

Funding

This work was performed on the bwUniCluster 3.0 supercomputer at the Scientific Computing Centre (SCC) of the Karlsruhe Institute of Technology, with support from the Ministry of Science, Research and the Arts Baden-Württemberg (Germany) and the German Federal Ministry of Education and Research, under project 'bwHPC-S5: Scientific Simulation and Storage Support Services'.

ORCID

Thorsten Zirwes http://orcid.org/0000-0002-3563-1422

References

[1] T. Lundgren, *Linearly Forced Isotropic Turbulence*. Annual Research Briefs, Center for Turbulence Research, Stanford University, Stanford, CA (2003). p. 461–473

[2] C. Rosales and C. Meneveau, *Linear forcing in numerical simulations of isotropic turbulence: physical space implementations and convergence properties*. Phys Fluids 17 (2005), p. 095106. doi:10.1063/1.2047568.

[3] P.L. Carroll and G. Blanquart, *A proposed modification to Lundgren's physical-space velocity forcing method for isotropic turbulence*. Phys Fluids 25 (2013), pp. 105–114. doi:10.1063/1.4826315.

[4] M. Bassenne, J. Urzay, G.I. Park and P. Moin, *Constant-energetics physical-space forcing methods for improved convergence to homogeneous-isotropic turbulence with application to*

particle-laden flows. Phys Fluids 28 (2016), p. 035114. doi:10.1016/j.ijmultiphaseflow.2019.04.025.

[5] B. de Laage de Meux, B. Audebert, R. Manceau and R. Perrin, *Anisotropic linear forcing for synthetic turbulence generation in LES and hybrid RANS/LES modeling*. Phys Fluids 27 (2015), p. 035115. doi:10.1063/1.4916019.

[6] J.A. Denev, T. Zirwes, F. Zhang and H. Bockhorn, *A low-pass filter for linear forcing in the open-source code OpenFOAM – implementation and numerical performance*, in *High Performance Computing in Science and Engineering '21. HPCSE 2021*, Nagel W.E., Kröner D.H., Resch M.M., eds., Springer, Cham, 2023. pp. 339–352. doi:10.1007/978-3-031-17937-2_20

[7] H.G. Weller, G. Tabor, H. Jasak and C. Fureby, *A tensorial approach to computational continuum mechanics using object-oriented techniques*. Comput Phys 12(6) (1998), pp. 620–631. doi:10.1063/1.168744.

[8] S.B. Pope, *Turbulent flows*, Cambridge University Press, Cambridge, 2000.

[9] P. Moin and K. Mahesh, *Direct numerical simulation: a tool in turbulence research*. Annu Rev Fluid Mech 30 (1998), pp. 539–578. doi:10.1146/annurev.fluid.30.1.539.

[10] T. Nilsson, H. Carlsson, R. Yu and X.-S. Bai, *Structures of turbulent premixed flames in the high Karlovitz number regime – DNS analysis*. Fuel 216 (2018), pp. 627–638. doi:10.1016/j.fuel.2017.12.046.

[11] R. Yu, X.-S. Bai and A.N. Lipatnikov, *A direct numerical simulation study of interface propagation in homogeneous turbulence*. J. Fluid Mech 772 (2015), pp. 127–164. doi:10.1017/jfm.2015.211.

[12] R. Courant, K. Friedrichs and H. Lewy, *Über die partiellen Differenzengleichungen der mathematischen Physik*. Math. Annal. 100(1) (1928), pp. 32–74. doi:10.1007/BF01448839.

[13] M. Klein and N. Chakraborty, Relation between 3 and 2D wrinkling factors in turbulent premixed flames. Flow Turbul Combust 114 (2024), pp. 519–526. doi:10.1007/s10494-024-00622-7.

[14] C. Bedoya, I. Dinkov, P. Habisreuther, N. Zarzalis, H. Bockhorn and P. Parthasarathy, *Experimental study, 1D volume-averaged calculations and 3D direct pore level simulations of the flame stabilization in porous inert media at elevated pressure*. Combust Flame 162 (2015), pp. 3740–3754. doi:10.1016/j.combustflame.2015.07.012.

[15] R.J. Kee, M.E. Coltrin and P. Glarborg, *Chemically reacting flow: theory and practice*, John Wiley & Sons, Hoboken, 2005.

[16] T. Zirwes, M. Sontheimer, F. Zhang, A. Abdelsamie, F.E. Hérnandez Pérez, O.T. Stein, H.G. Im, A. Kronenburg and H. Bockhorn, *Assessment of numerical accuracy and parallel performance of OpenFOAM and its reacting flow extension EBIdnsFoam*. Flow Turbul Combust 111 (2023), pp. 567–602. doi:10.1007/s10494-023-00449-8.

[17] D.G. Goodwin, H.K. Moffat, I. Schoegl, R.L. Speth and B.W. Weber, Cantera: an object-oriented software toolkit for chemical kinetics, thermodynamics, and transport processes. https://www.cantera.org. Version 3.1.0 (2024)

[18] T. Poinsot and D. Veynante, *Theoretical and numerical combustion*, R.T. Edwards, Inc., Philadelphia, PA, 2005. 522 p.

[19] M. Klein, N. Chakraborty and S. Ketterl, *A comparison of strategies for direct numerical simulation of turbulence chemistry interaction in generic planar turbulent premixed flames*. Flow, Turbul Combust 99(3-4) (2017), pp. 955–971. doi:10.1007/s10494-017-9843-9.

[20] J.A. Palmore and O. Desjardins, *Technique for forcing high Reynolds number isotropic turbulence in physical space*. Phys. Rev. Fluids 3 (2018), pp. 034605. doi:10.1103/PhysRevFluids.3.034605.